Journal of Power Sources 249 (2014) 405–413

Contents lists available at ScienceDirect

Journal of Power Sources

journal homepage: www.elsevier.com/locate/jpowsour

High valence transition metal doped strontium ferrites for electrode materials in symmetrical SOFCs

A.J. Fernández-Ropero [a,b], J.M. Porras-Vázquez [c], A. Cabeza [a], P.R. Slater [c], D. Marrero-López [d], E.R. Losilla [a,*]

[a] Department of Inorganic Chemistry, University of Malaga, 29071 Málaga, Spain
[b] CIC energiGUNE, Parque Tecnológico de Álava, Albert Einstein 48, 0150 Miñano, Spain
[c] School of Chemistry, University of Birmingham, Birmingham B15 2TT, UK
[d] Department of Applied Physics I, Laboratory of Materials and Surfaces, University of Málaga, 29071 Málaga, Spain

HIGHLIGHTS

- Doped $SrFeO_{3-\delta}$ perovskite materials have been prepared by a freeze-drying method.
- High valance transition metals can be incorporated into $SrFeO_{3-\delta}$ with cubic symmetry.
- Chemical compatibility of $SrFe_{0.75}M_{0.25}O_{3-\delta}$ with CGO and LSGM showed no reactivity.
- ASR values of 0.09 and 0.41 Ω cm^2 at 800 °C were obtained for $SrFe_{0.75}Nb_{0.25}O_{3-\delta}$ in air and 5% H_2–Ar respectively.
- $SrFe_{0.75}M_{0.25}O_{3-\delta}$ are suitable as both cathode and anode materials in symmetrical SOFCs.

ARTICLE INFO

Article history:
Received 25 July 2013
Received in revised form
2 October 2013
Accepted 21 October 2013
Available online 4 November 2013

Keywords:
Symmetrical SOFC
Transition metal
Cathode and anode material
$SrFeO_{3-\delta}$

ABSTRACT

In this paper we report the successful incorporation of high valence transition metals, i.e. Cr, Mo, W, V, Nb, Ti, Zr into $SrFeO_{3-\delta}$ perovskite materials, for potential applications as symmetric electrode materials for Solid Oxide Fuel Cells. It is observed that the doping leads to a change from an orthorhombic structure (with partial ordering of oxygen vacancies) to a cubic one (with the oxygen vacancies disordered). These electrodes are chemically compatibles with $Ce_{0.9}Gd_{0.1}O_{1.95}$ (CGO) and $La_{0.8}Sr_{0.2}Ga_{0.8}Mg_{0.2}O_{3-\delta}$ (LSGM) electrolytes at least up to 1100 °C. Thermal annealing experiments in 5% H_2–Ar at 800 °C also show the stability of the doped samples in reducing conditions, suggesting that they may be suitable for both cathode and anode applications. In contrast, reduction of undoped $SrFeO_{3-\delta}$ leads to the observation of extra peaks indicating the formation of the brownmillerite structure with the associated oxygen vacancy ordering. The performance of these electrodes was examined on dense electrolyte pellets of CGO and LSGM in air and 5% H_2–Ar. In both atmospheres an improvement in the area specific resistances (ASR) values is observed for the doped samples with respect to the parent compound. Thus, the results show that high valence transition metals can be incorporated into $SrFeO_{3-\delta}$-based materials and can have a beneficial effect on the electrochemical performance, making them potentially suitable for use as cathode and anode materials in symmetrical SOFC.

1. Introduction

Solid Oxide Fuel Cells (SOFCs) are electrochemical devices with higher efficiency for electrical generation than conventional systems based on fuel combustion. SOFCs have several advantages compared to other fuel cells types, such as relatively lower costs, greater tolerance to impurities in the fuel and the possibility to operate directly on hydrocarbon fuels [1–5].

A typical SOFC consists of three main ceramic components, i.e. an anode, a cathode and a solid electrolyte. The state-of-the-art solid electrolyte is $Zr_{0.84}Y_{0.16}O_{1.92}$ (YSZ) and the cathode $La_{1-x}Sr_xMnO_{3-\delta}$ (LSM)/YSZ composite. The anode material is usually a composite of Ni and the electrolyte, which exhibits excellent electrocatalytic properties for operation in H_2 fuel. However, this anode does have certain disadvantages; in particular those related

* Corresponding author. Dpto. de Química Inorgánica, Universidad de Málaga, 29071 Málaga, Spain. Tel.: +34 952134234; fax: +34 952131870.
E-mail address: r_losilla@uma.es (E.R. Losilla).

0378-7753/$ – see front matter © 2013 Elsevier B.V. All rights reserved.
http://dx.doi.org/10.1016/j.jpowsour.2013.10.118

to carbon deposition when operating with hydrocarbon fuels, sulphur poisoning, agglomeration of Ni particles and volume instability upon redox cycling [6,7]. This traditional SOFC configuration may be replaced by a new approach, where the same electrode material could be used simultaneously as both cathode and anode to create a symmetrical solid oxide fuel cells. Symmetrical Solid Oxide Fuel Cells (SSOFC) present several advantages compared to conventional SOFCs, because the number of cell components is reduced facilitating the assembly of a fuel cell in a single thermal treatment and minimizing compatibility requirements [8–10]. Furthermore, this configuration could overcome two of the main drawbacks associated to SOFC technology when operating directly with hydrocarbon fuels, i.e. reversible sulphur poisoning and carbon deposition, due to the possibility to reverse the gas flow oxidizing any sulphur species or C-deposit and hence recovering any loss of performance.

In the last few years there has been a growing interest in the research of potential symmetrical electrode materials for SOFC applications, such as $La_{0.75}Sr_{0.25}Cr_{0.5}Mn_{0.5}O_{3-\delta}$ (LSCM), $La_{1/3}Sr_{2/3}(Ti_{1-x}Fe_x)O_{3-\delta}$, and $Sr_2Fe_{1.5}Mo_{0.5}O_{6-\delta}$ [8,11,12].

The perovskites based on $SrFeO_{3-\delta}$ are interesting materials which exhibit high mixed oxide ionic and electronic conductivity and therefore can be potentially used as both cathode and anode material in SSOFCs [13–15]. Iron cations in this system are in a mixed oxidation states ranging from +4 to +3, corresponding to a wide range of oxygen nonstoichiometry. Over the oxygen composition range $2.5 \leq 3-\delta \leq 3$, the $SrFeO_{3-\delta}$ system exits as four distinct compounds with the nominal composition $Sr_nFe_nO_{3n-1}$ (n = 2, 4 and 8). The end member $SrFeO_3$ ($n = \infty$) possesses a simple cubic perovskite crystal structure, whereas the oxygen-deficient (n = 2, 4 and 8) members adopt different vacancy-ordered perovskite crystal structures from brownmillerite-type (n = 2) to orthorhombic *Cmmm* (n = 4) and tetragonal *I4/mmm* (n = 8) [16–18]. The formation of ordered oxygen vacancies is not favourable for practical applications because it drastically reduces oxide ion conduction, whilst the oxygen deficiency also results in a decrease in both mobility and concentration of hole carriers [19,20].

The aim of this work is to investigate high valence transition metal doping into $SrFeO_{3-\delta}$ systems, with a view to stabilize the cubic form of these systems, avoiding the phase transition to the brownmillerite form and improving the electrochemical performance as anode and cathode material in SSOFCs.

2. Experimental

2.1. Synthesis and powder characterization

$SrFe_{0.75}M_{0.25}O_{3-\delta}$ (M = Ti, Zr, V, Nb, Cr, Mo, W) series and the undoped sample $SrFeO_3$ (SFO), were prepared by freeze-drying of an aqueous cation solution. The starting reagents for the syntheses were: $Sr(NO_3)_2$ (99.9%, Aldrich), $Fe(NO_3)_3{\cdot}9H_2O$ (98%, Alfa-Aesar), $Cr(NO_3)_3{\cdot}9H_2O$ (99%, Aldrich), MoO_3 (99.5%, Aldrich), WO_3 (99.5%, Aldrich), NH_4VO_3 (99.9%, Alfa-Aesar), $Nb(HC_2O_4)_5{\cdot}H_2C_2O_4$ (97%, ABCR), $Ti[OCH(CH_3)_2]_4$ (99%, Aldrich) and $ZrO(NO_3)_2{\cdot}6H_2O$ (99%, Aldrich). Cation solutions were prepared separately dissolving the metal nitrates in distilled water, while the oxides WO_3 and MoO_3 were dissolved in diluted ammonia. The solutions were mixed in stoichiometric amounts and ethylenediaminetetraacetic acid (EDTA) (99.5% Aldrich) was added as complexing agent in a 1:1 ligand:metal molar ratio. The pH was adjusted to approximately 7 with the addition of ammonia. The resulting solutions were frozen by dropwise addition into liquid nitrogen and the frozen drops were dehydrated by vacuum sublimation in a freeze-drier for 2 days obtaining an amorphous solid precursor. The precursor powders were immediately heated at 300 °C to avoid the rehydration and to produce the combustion of organic material. Afterwards, the powders were fired at 800 °C to remove the carbonaceous species and to achieve crystallization.

X-ray powder diffraction (XRPD) measurements were performed to study the purity of the samples, crystal structure, reactivity with different electrolytes and the chemical stability under very reducing atmospheres.

For the chemical compatibility studies, the ferrites and commercial electrolyte powders, $Ce_{0.9}Gd_{0.1}O_{2-\delta}$ (CGO, Pi-Kem) and $La_{0.8}Sr_{0.2}Ga_{0.8}Mg_{0.2}O_{3-\delta}$ (LSGM, Praxair), were mixed in a 1:1 weight ratio in an agate mortar and then fired in air at 1100 °C for 24 h. The powder mixtures were then slowly cooled down to room temperature and examined by XRPD. The phase stability of the materials in very reducing atmospheres was evaluated exposing the powder under a constant flow of 5% H_2–Ar at 800 °C for 24 h.

The XRPD patterns were collected using a PANalytical X'Pert Pro automated diffractometer equipped with a Ge(111) primary monochromator (Cu $K\alpha_1$) and a X'Celerator detector in the 2θ range (10–140°) with 0.016° step size for 1–4 h. Rietveld analyses were done using the GSAS suite of programmes [21] and phase identification was performed with X'Pert HighScore Plus v.2.0e software using the ICSD database for the starting structural models [22,23]. The usual profile parameters (scale factors, background coefficients, zero-points, pseudo-Voigt, asymmetry for the peak-shape and atomic parameters) were fitted.

X-ray photoelectron spectroscopy (XPS) measurements were carried out to evaluate the oxidation states of the dopants in the oxidized and reduced samples. XPS spectra were recorded on a Physical Electronics PHI-5700 spectrometer equipped with Mg-K_α and Al-K_α X-ray sources and a hemispherical analyser. The data were analysed using PHI ACCES ESCA-V6.0 F software. The experimental peaks were decomposed into components using mixed Gaussian–Lorentzian functions. The binding energies (BE) were referenced to the adventitious carbon C(1s) at 284.4 eV.

2.2. Electrical measurements

Ceramic pellets of doped-$SrFeO_{3-\delta}$, CGO and LSGM ($\sim$13 mm of diameter and $\sim$1 mm of thickness) were obtained by pressing the powder at 75 MPa. The pellets were sintered at a heating rate of 10 °C min^{-1} at 1250 °C (doped-$SrFeO_{3-\delta}$) and 1400 °C (CGO and LSGM) for 4 h. Conductivity measurements were performed using the four probe dc method for the electrode materials. Four Pt electrodes were attached with Pt paste, and then the sample was fired to 800 °C in air for 1 h to ensure bonding to the sample. The electrical measurements were carried out in air and 5% H_2–Ar during the cooling process with a dwell time of 1 h at each temperature. The samples were previously treated at 800 °C for several hours in air and 5% H_2–Ar. The conductivity was not corrected for the influence of porosity due to the high relative density of the samples >90%.

Area specific polarization resistance (ASR) values were obtained under symmetrical atmospheres (without chemical potential gradient) in a two electrode configuration. The electrode powders were mixed in a 50 wt.% with Decoflux™ (WB41, Zschimmer and Schwarz) as binder material to obtain a slurry which was used to paint symmetrical electrodes on dense pellets of CGO and LSGM electrolyte. The electrodes were sintered at 1100 °C for 1 h to ensure an adequate adherence with the electrolyte. The symmetrical cells were measured by impedance spectroscopy in air and under a continuous flow of humidified 5% H_2–Ar using a 1260 Solartron FRA in the 0.1–10^6 Hz frequency range from 800 to 500 °C with a cooling rate of 5 °C min^{-1} and a stabilization time of 30 min between measurements. An ac signal of 50 mV was applied. Pt-ink

electrodes were used as current collectors and the data were analysed with ZView software [24].

The microstructure of the sintered pellets and cross-section of the electrolyte/electrode interfaces were examined by Scanning Electron Microscopy (SEM) by using a JEOL SM-6490LV. The samples for SEM observation were gold sputtered to reduce charging of the surface.

3. Results and discussions

3.1. Phase formation

Precursor powders of SFO and $SrFe_{0.75}M_{0.25}O_{3-\delta}$ (M = Ti, Zr, V, Nb, Cr, Mo, W) series were fired between 800 and 1250 °C for 5 h to obtain highly crystalline materials. $SrFeO_{3-\delta}$ and the samples doped with W and Ti were single phase materials at 800 °C, and an increase of the temperature up to 1250 °C only led to more crystalline compounds (Fig. 1a and b). Cr and Mo-doped samples were single phase materials at 1000 °C. At lower temperatures, secondary phases of $SrCrO_4$ and $SrMoO_4$ were formed (Fig. 1c and d) as secondary phases. For the Nb and Zr-doped samples, the temperature needed to achieve a single phase sample was 1100 °C, while below this temperature secondary phases were detected (Fig. 1e and f). The V-doped sample was a mixture of phases in the whole temperature range studied 800–1250 °C. Three crystalline phases $SrFeO_3$, $Sr_3(VO_4)_2$ and $Sr_3Fe_2O_6$ were found after calcining at 1250 °C for 5 h. Thus, it was not possible to achieve a single phase at any temperature, and therefore V-doped sample was not analysed further.

3.2. Structural characterization

The crystal structures of the samples were analysed using the Rietveld method. The structure of $SrFeO_{3-\delta}$ was reported to be strongly related to the concentration and arrangement of oxygen vacancies, which depend on temperature and oxygen partial pressure [16]. Under our synthetic conditions, the structure of the undoped sample was indexed and refined in an orthorhombic perovskite cell with s.g. (space group) *Cmmm* (Table 1).

All transition metal doped compounds, $SrFe_{0.75}M_{0.25}O_{3-\delta}$ (M = Ti, Zr, Nb, Cr, Mo, W), are indexed in a cubic perovskite cell (*Pm-3m*). Assuming an octahedral coordination of the dopant in the B-site of the perovskite, the stabilization of the cubic form is likely due to the incorporation of a transition metal with high oxidation state (higher than oxidation states expected in the undoped sample, Fe^{3+} and Fe^{4+}) leading to the introduction of oxide anions to compensate the positive charge and stabilizing the cubic form (see Fig. 2b for $SrFe_{0.75}Ti_{0.25}O_{3-\delta}$).

Refined cell parameters obtained by the Rietveld method are given in Table 1. In these compounds it is difficult to correlate the cell volume with the cation size (using Shannon ionic radius). This is likely due to the different oxygen contents caused by the replacement of iron by transition metals with different oxidation states, in addition to changes in the valence of iron to maintain the charge neutrality requirement. Further studies by thermogravimetric analysis and neutron diffraction are necessary to determine the oxygen stoichiometry in these samples.

It should be also commented that Ti-substitution in $SrFeO_3$ produces a smaller change of the unit volume cell compared to the

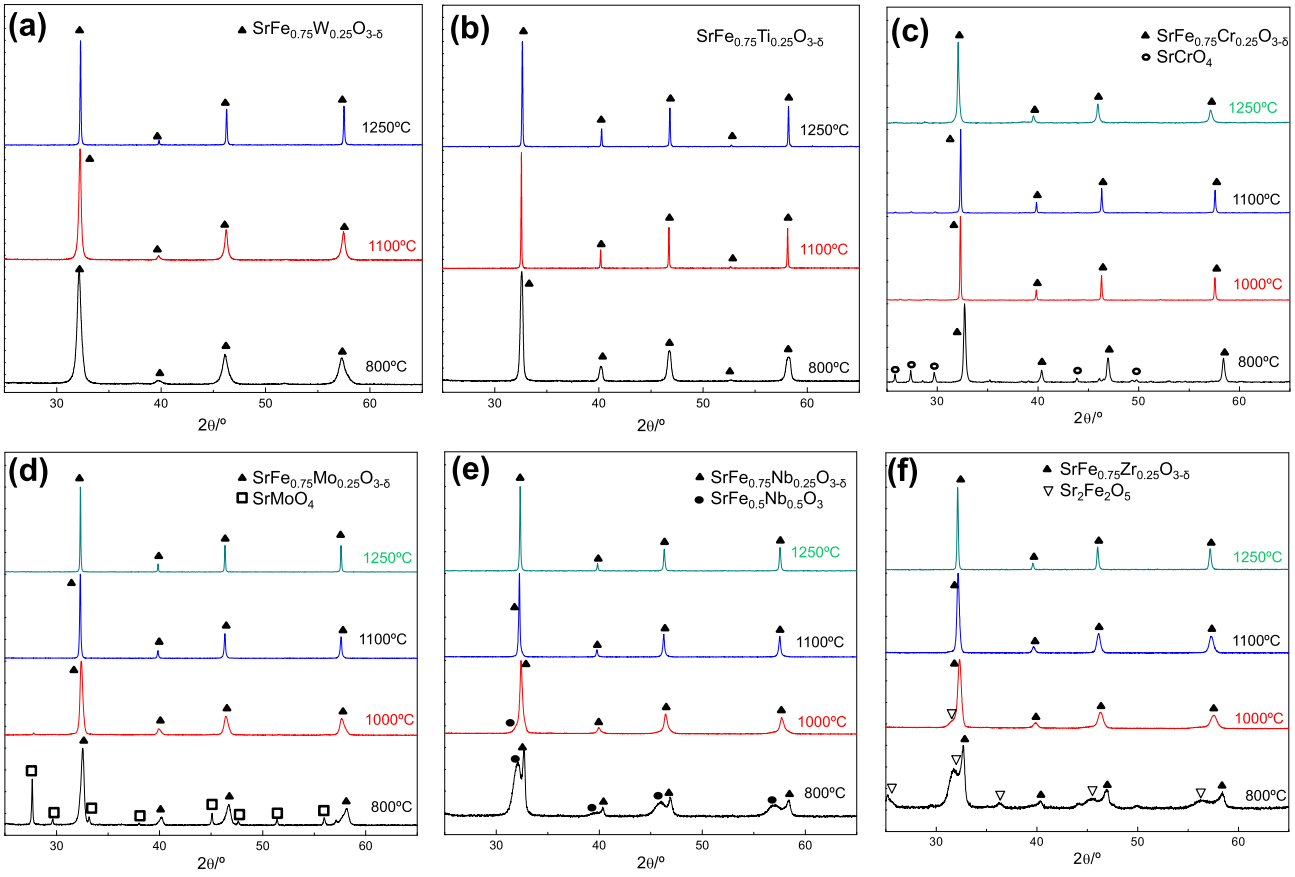

Fig. 1. XRPD patterns for (a) $SrFe_{0.75}W_{0.25}O_{3-\delta}$, (b) $SrFe_{0.75}Ti_{0.25}O_{3-\delta}$, (c) $SrFe_{0.75}Cr_{0.25}O_{3-\delta}$, (d) $SrFe_{0.75}Mo_{0.25}O_{3-\delta}$, (e) $SrFe_{0.75}Nb_{0.25}O_{3-\delta}$ and (f) $SrFe_{0.75}Zr_{0.25}O_{3-\delta}$ fired at 800 °C for 1 h; and at 1100 °C and 1250 °C for 5 h.

Table 1
Unit cell parameters, Rietveld disagreement factors, compaction and average grain size D_g for $SrFe_{0.75}M_{0.25}O_{3-\delta}$ (M = Ti, Zr, Nb, Cr, Mo and W) series in the space group *Pm-3m*.

M	Cell parameters (Å)	V/Z (Å^3)	R_{wp} (%)	R_F (%)	Compaction (%)	D_g (μm)
Fe[a]	$a = 10.97082(8)$ $b = 7.70653(5)$ $c = 5.47234(4)$	57.834(2)	7.42	7.31	90	14.2
Ti	3.88570(1)	58.669(0)	3.06	2.02	92	5.7
Zr	3.94868(3)	61.568(2)	2.35	1.39	92	2.0
Nb	3.92701(2)	60.560(1)	1.97	2.05	92	1.1
Cr	3.9504(1)	61.648(6)	3.02	2.15	90	3.0
Mo	3.92086(1)	60.276(0)	2.50	1.86	93	1.4
W	3.92749(1)	60.582(0)	2.70	3.45	90	0.4

[a] $SrFeO_{3-\delta}$ crystallizes in the *Cmmm* orthorhombic space group.

parent compound, on the contrary, Zr-substitution leads to a large unit cell distortion. This has strong effects on the electrochemical properties as can be seen in the next sections.

3.3. Phase stability in H_2

The anode material of a SOFC should be structurally stable under reducing conditions. Thus, phase transformation or partial decomposition of the crystal structure is considered to be detrimental for practical application due to the possible volume change of the anode during the oxidation and reduction cycles, causing delamination of the cell layers.

The stabilities for the $SrFe_{0.75}M_{0.25}O_{3-\delta}$ (M = Ti, Zr, Nb, Cr, Mo, W) series were investigated by XRPD after a thermal treatment of the powders in a 5% H_2–Ar flow at 800 °C for 24 h. The XRPD patterns for undoped $SrFeO_{3-\delta}$ and $SrFe_{0.75}Cr_{0.25}O_{3-\delta}$ indicated that both materials show significant changes at 800 °C (Fig. 3), with the appearance of the reflections of the brownmillerite phase $Sr_2Fe_2O_{5-\delta}$. This is due to partial reduction of Fe and Cr to lower oxidation states with the subsequent oxygen loss. This process entails the ordering of the oxygen vacancies and the formation of the brownmillerite phase with orthorhombic symmetry. On the other hand, $SrFe_{0.75}M_{0.25}O_{3-\delta}$ (M = Ti, Zr, Nb, Mo and W) were shown to be structurally stable under reducing atmosphere at 800 °C (Fig. 3) maintaining a cubic lattice; therefore these samples could have potential as anode materials.

3.4. Chemical compatibility

The reactivity between the electrolyte and the electrode layers is another important issue to be considered in the fabrication of an SOFC due to the fact that the formation of new phases or even a low ionic conducting material at the interface between both materials might increase significantly the ohmic resistance of the cell and block partially the oxygen transport. On the other hand, a poor electrode adherence might result in a large contact resistance and even delamination of both layers. For these reasons, it is essential to know the optimum fixing temperature, minimizing the possible formation of reaction products at the interface between the electrode and electrolyte layers.

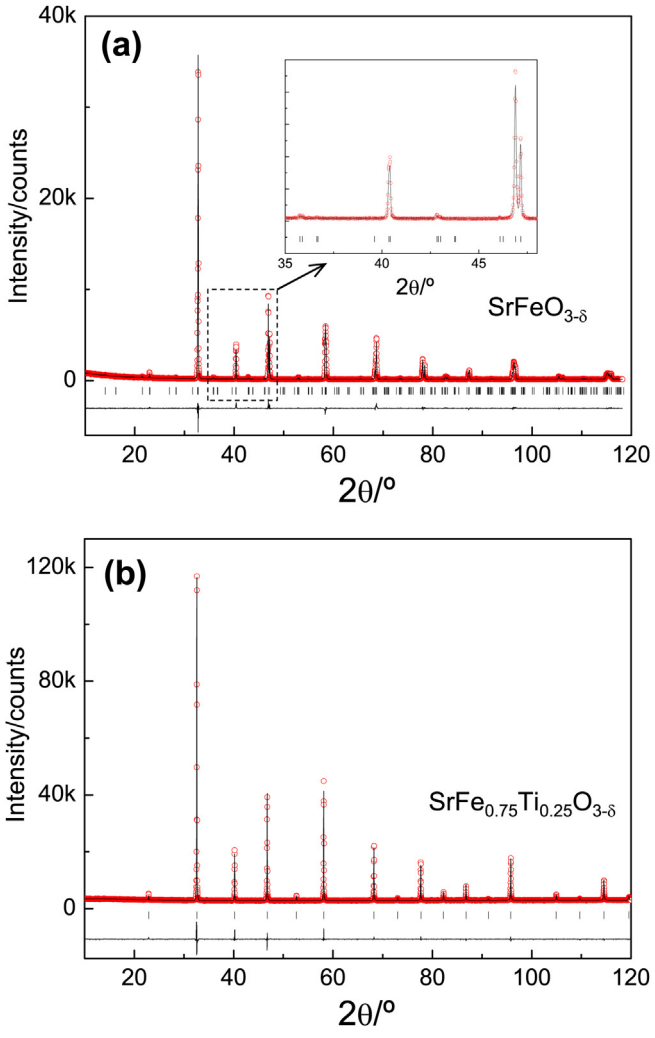

Fig. 2. Rietveld plots [observed data (circles), calculated pattern (full line), and difference curve (bottom)] for (a) orthorhombic (s.g. *Cmmm*) $SrFeO_{3-\delta}$ and (b) cubic (s.g. *Pm-3m*) $SrFe_{0.75}Ti_{0.25}O_{3-\delta}$.

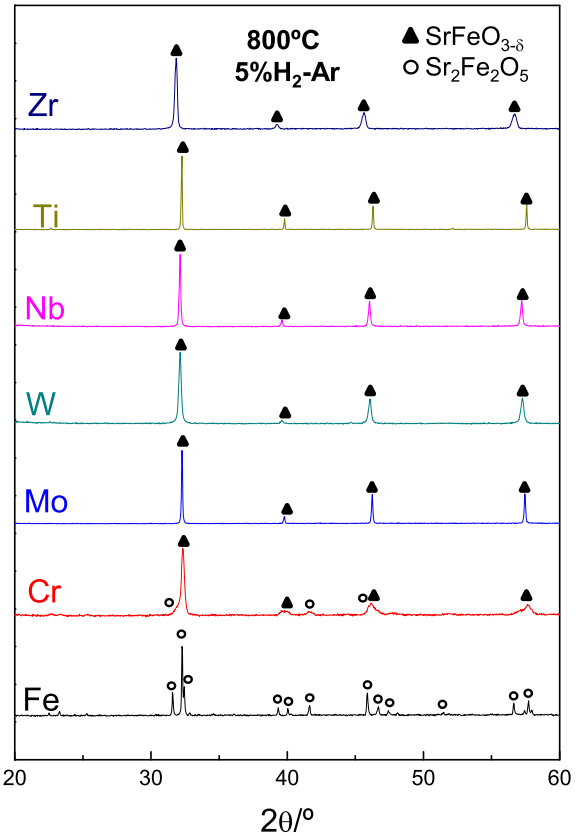

Fig. 3. XRPD patterns for $SrFe_{0.75}M_{0.25}O_{3-\delta}$ (M = Ti, Zr, Nb, Cr, Mo, W) after firing at 800 °C under 5% H_2–Ar.

The XRPD patterns of the mixtures of SFO and $SrFe_{0.75}M_{0.25}O_{3-\delta}$ (M = Ti, Zr, Nb, Cr, Mo and W) electrodes with LSGM and CGO electrolytes are shown in Figs. 4 and 5, respectively. These electrodes and electrolytes seem to be chemically compatible up to 1100 °C. Only for the $SrFe_{0.75}Zr_{0.25}O_{3-\delta}$/CGO mixture was a small unidentified impurity at $2\theta = 31°$ observed (Fig. 5f).

While a possible interdiffusion of cations between the materials is not ruled out, the cell parameters of the different phases did not change appreciably after annealing the powder mixture at 1100 °C.

3.5. Sintering conditions and microstructure

The sintering conditions used for the preparation of SFO and $SrFe_{0.75}M_{0.25}O_{3-\delta}$ (M = Ti, Zr, Nb, Cr, Mo and W) ceramic pellets at 1250 °C 4 h led to dense specimens with compactions ranging from 90% to 95% of the theoretical value, taking into account the pellet mass and volume and the crystallographic density (Table 1). Fig. 6 shows representative SEM micrographs for the dense pellets. All ceramic materials have low porosity with no indication of liquid phase formation or phase segregations at the grain boundaries. The SEM micrographs also reveal that the ceramic grain size is highly affected by the dopants. The average grain sizes *D* are given in Table 1. As can be observed, the undoped composition, $SrFeO_{3-\delta}$, exhibits the largest grain size (14.2 μm), however, smaller grain sizes are observed in the doped samples. This is usually attributed to an enrichment of the dopant at the grain boundary region as previously observed for other ceramic materials [25]. According to the space charge model, the excess of dopant located at the grain boundary retains the mobility of cations across this region and consequently, the grain growth rate decreases. It is difficult to relate the grain size with the dopant type due to the different oxidation states of these samples; however, those samples containing higher valence transition metal dopants, i.e. W^{6+} and Mo^{6+}, seem to exhibit the lowest grain size (Fig. 6e and f and Table 1). Samples with different dopant content should be studied to explain this behaviour.

3.6. X-ray photoelectron spectroscopy

The different electronic conductivity under oxidizing and reducing conditions in these materials is related to the change in the valence of the cations in B-site caused by oxygen losses with the temperature and the oxygen partial pressure. For this reason, ceramic pellets before and after reduction in 5% H_2–Ar atmosphere for 24 h were examined by XPS to evaluate the different valence of the cations and to obtain new insights on the electronic conduction.

The XPS survey for the different samples treated in air and 5% H_2–Ar indicates that the surface of the powders is enriched in Sr (~70 atom% in air) and depleted in dopant ~7 atom% due to the presence of strontium carbonate.

Fig. S3a and b shows the C1s spectra for Mo-containing sample with two separated peaks and at least five different contributions for all the samples. They have been ascribed to adventitious carbon, different C–O and C=O species and carbonates, being those corresponding to C–O and carbonates the most intense ones for the oxidized samples (Fig. S3a). In contrast, the carbonate content is lower in those samples treated under 5% H_2–Ar (Fig. S3b).

The W 4f, Nb 3d and Ti 2p core levels of the dopants show similar features in both oxidizing and reducing atmospheres (Fig. S4a–f). The spectra of the reduced samples are slightly shifted to higher binding energies compared to the oxidised ones, which is explained by the different conductivity values of these samples in

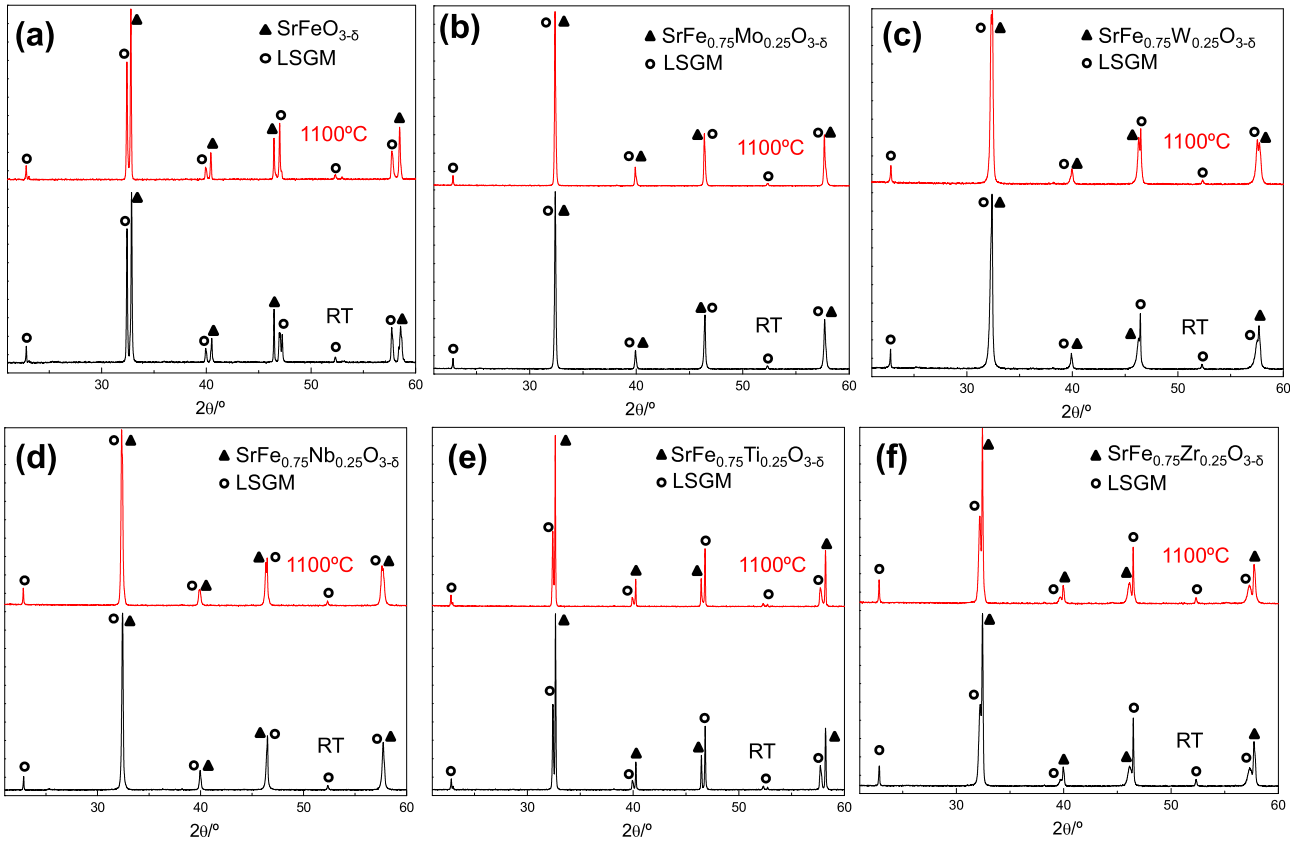

Fig. 4. XRPD patterns for a) $SrFeO_{3-\delta}$/LSGM, b) $SrFe_{0.75}Mo_{0.25}O_{3-\delta}$/LSGM, c) $SrFe_{0.75}W_{0.25}O_{3-\delta}$/LSGM, d) $SrFe_{0.75}Nb_{0.25}O_{3-\delta}$/LSGM, e) $SrFe_{0.75}Ti_{0.25}O_{3-\delta}$/LSGM and f) $SrFe_{0.75}Zr_{0.25}O_{3-\delta}$/LSGM mixtures (1:1 wt.%) at room temperature (RT) and after firing at 1100 °C for 24 h in air.

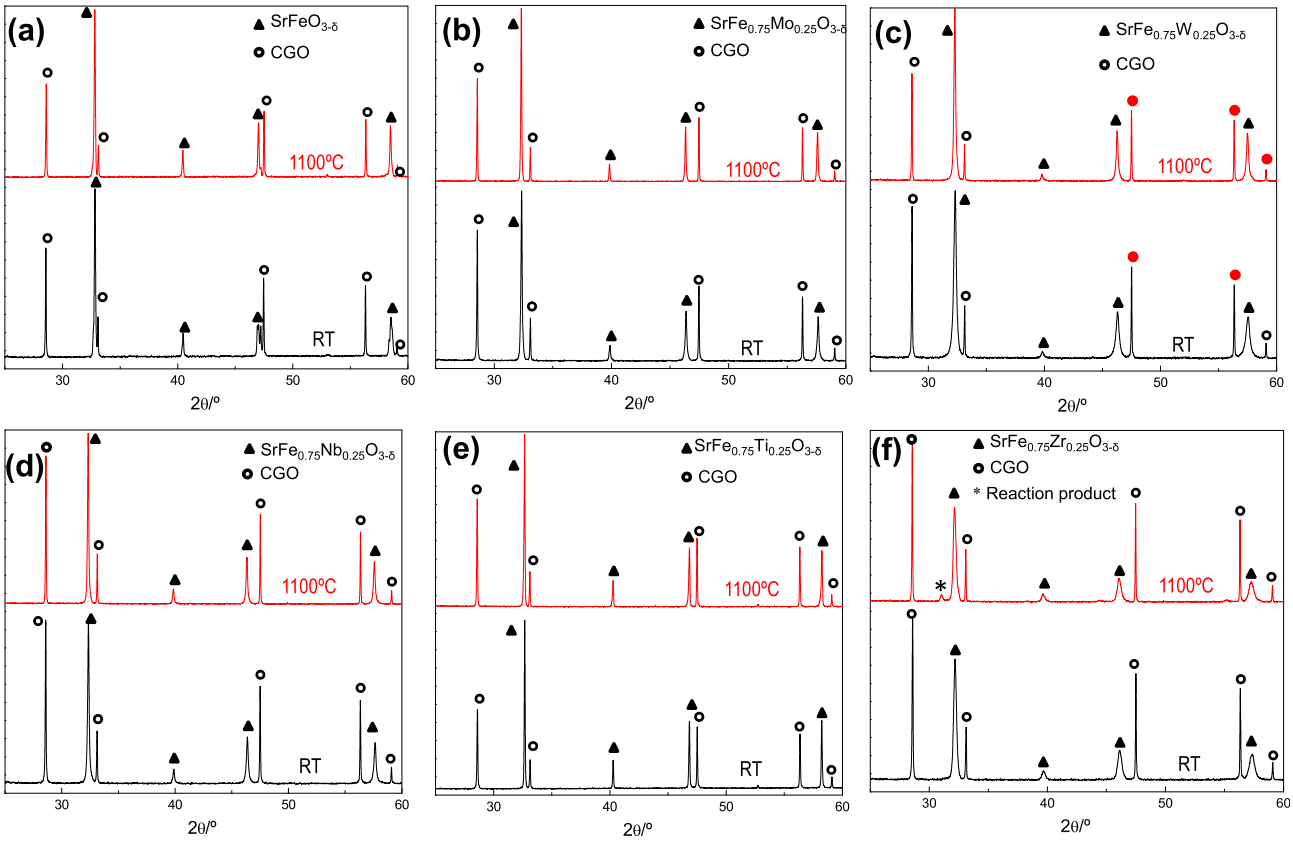

Fig. 5. XRPD patterns for a) $SrFeO_{3-\delta}$/CGO, b) $SrFe_{0.75}Mo_{0.25}O_{3-\delta}$/CGO, c) $SrFe_{0.75}W_{0.25}O_{3-\delta}$/CGO, d) $SrFe_{0.75}Nb_{0.25}O_{3-\delta}$/CGO, e) $SrFe_{0.75}Ti_{0.25}O_{3-\delta}$/CGO and f) $SrFe_{0.75}Zr_{0.25}O_{3-\delta}$/CGO mixtures (1:1 wt.%) at room temperature (RT) and after firing at 1100 °C for 24 h in air.

reducing and oxidizing atmospheres. The characteristic doublets of these signals were fitted by considering only one contribution with binding energies of 35.2, 206.2 and 457 eV for W $4f_{7/2}$, Nb $3d_{3/2}$ and Ti $2p_3/_2$ respectively, which are assigned to W^{6+}, Nb^{5+} and Ti^{4+}. Thus, it was impossible to quantify the different oxidation states of the dopants in reducing atmosphere due to the superficial carbonation and oxidation of the samples in contact with air before acquired the XPS spectra.

Only Mo 3d core level shows a different behaviour (Fig. S4g and h). This spectrum was fitted considering two doublets with binding energy values of 232.2 and 231.7 eV, indicating the presence of molybdenum in different oxidation states or alternatively a minor and superficial secondary phase. The sample exposed to air shows a significant increase of the lower binding energy contribution (Fig. S4h) compared to that treated in H_2 atmosphere (Fig. S4g). This contribution can not be attributed to the presence of molybdenum

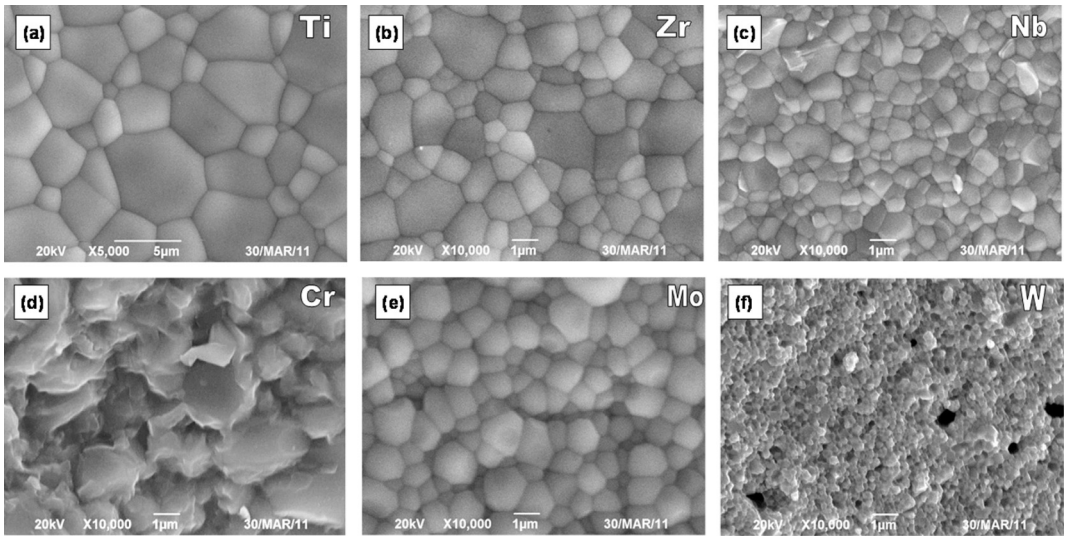

Fig. 6. SEM micrographs for $SrFe_{0.75}M_{0.25}O_{3-\delta}$ pellets with M= a) Ti, b) Zr, c) Nb, d) Cr, e) Mo and f) W sintered at 1250 °C for 4 h.

with lower valence, i.e. $Mo^{5+,4+}$, because this is expected to increase under reducing conditions. Hence, this is possibly associated to superficial segregation after exposed the samples in air atmosphere, e.g. $SrMoO_4$, as previously observed in related perovskites Sr_2FeMoO_6 and Sr_2MgMoO_6 [26,27].

3.7. Electrical conductivity

The temperature dependence of the conductivity of these phases in air and 5% H_2–Ar is shown in Fig. 7. According to the literature data, the conductivity of undoped $SrFeO_3$ is sensitive to the oxygen content and oxygen partial pressure, it shows p-type conducting behaviour under oxygen partial pressures above 10^{-5} atm and predominant n-type conduction below 10^{-15} atm at 800 °C [18].

The high valence transition metal doping in $SrFeO_3$ leads to a decrease of the charge carrier Fe^{4+} in air, which also results in a decrease in conductivity (Fig. 7a). In air, all doped materials present semiconductor-type behaviour between room temperature and 600 °C, according to the small polaron conduction mechanism. Above this temperature a drop in the conductivity is observed, which is related to the thermal reduction of Fe^{4+} to lower valence states and the consequent decrease in the number of charge carriers, as reported for other iron-containing perovskites [12,28,29]. The highest conductivity value was found for $SrFe_{0.75}Ti_{0.25}O_{3-\delta}$, which is possibly related to the lowest distortion of the perovskite structure after doping compared to the parent compound ~40 S cm^{-1} at 600 °C, and the lowest one for $SrFe_{0.75}Zr_{0.25}O_{3-\delta}$, ~10 S cm^{-1} at the same temperature, with the largest distortion of the lattice structure after Zr-substitution (Table 1) and the stable oxidation state of Zr^{4+}, limiting the conduction by polaron hopping between iron ions.

The conductivity in hydrogen atmosphere for the undoped compound SFO is rather low due to the phase transformation to $Sr_2Fe_2O_5$ with low concentration of charge carriers Fe^{4+}. The conductivity of the doped samples is substantially higher compared to undoped one, evidencing the structural stability of the doped samples to reduction (Fig. 7b). The largest values of conductivity are found for the samples doped with high valence cations, i.e. 1 and 5 S cm^{-1} for W and Mo-doping respectively at 800 °C. The better conductivity of Mo-containing samples compared to tungsten seems to arise from the easy reduction of Mo^{6+} to lower oxidation states compared to W^{6+}. This indicates that the molybdenum cations in reducing conditions may acquire mixed 5+ and 6+ oxidation states and, thus, take part in electron transport, whereas the reduction of tungsten is lower and the electronic conductivity decreases substantially in the low temperature range. Similar observations are known for lanthanum tungstate and molybdates [30]. The lowest values of conductivity in hydrogen atmosphere were found for Zr^{4+} with stable oxidation state.

It should be also commented that the values of conductivity of these materials under reducing conditions are lower than those obtained under oxidizing atmosphere and therefore the efficiency operating as anode material is expected to be lower. This is a common feature of most of the symmetrical electrodes studied previously, e.g. $La_{0.75}Sr_{0.25}Cr_{0.5}Mn_{0.5}O_{3-\delta}$, which exhibits an electronic conductivity of only 0.5 S cm^{-1} at 800 °C in H_2 compared to 40 S cm^{-1} in air; however, high efficiency was obtained for this material operating in an SOFC as anode [31]. The addition of Cu is a useful method to improve the electronic conductivity, which is the main limiting factor for the practical application of these materials as anode [32].

3.8. Area specific resistance

Symmetrical cells of the different electrodes with LSGM and CGO electrolytes were prepared in order to study their electrochemical efficiencies as both cathode and anode in air and 5% H_2–Ar respectively. Fig. 8 displays representative SEM images of the LSGM/electrode interfaces. All electrodes showed a good adherence with the electrolyte and adequate porosity with well-connected grains. Reaction at the electrolyte/electrode interface was not observed in good agreement with XRPD results.

Representative impedance spectra in air and 5% H_2–Ar for several compositions are given as Supplementary material in Fig. S1. The equivalent circuit used to fit the spectra is comprised of an autoinductance (L), for the autoinductive processes of the equipment; a resistance (R), for all the ohmic losses; and two RQ elements for electrode processes: diffusion and charge transference. Fig. 9 displays the values of polarization resistances against the temperature for the different electrodes with LSGM electrolyte in air (Fig. 9a). It can be seen that for all the doped materials there is an improvement with respect to the undoped composition. For the LSGM electrolyte the best result is obtained for Ti-doping, with a

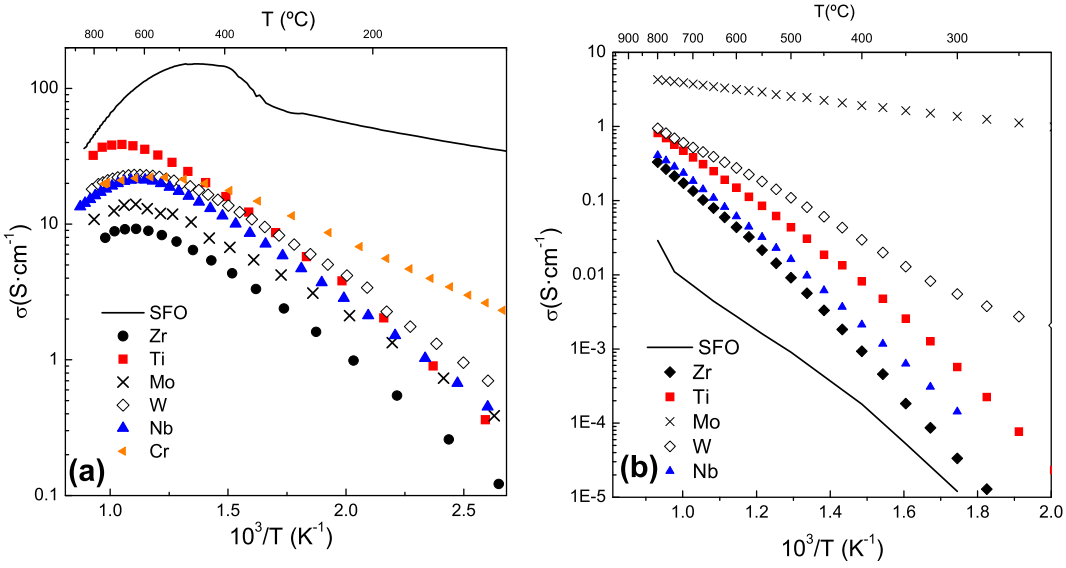

Fig. 7. Arrhenius plots of the conductivity for $SrFe_{0.75}M_{0.25}O_{3-\delta}$ (M = Ti, Zr, Nb, Cr, Mo, W) series: a) in air and b) in 5% H_2–Ar.

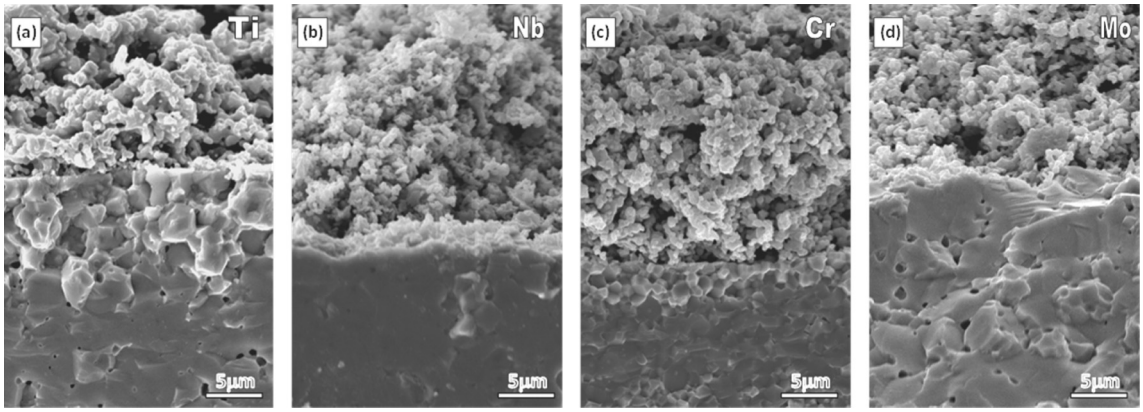

Fig. 8. SEM images of the cross-section of the $SrFe_{0.75}M_{0.25}O_{3-\delta}$/LSGM interface for a) Ti, b) Nb, c) Cr and d) Mo.

value of 0.25 Ω cm^2 at 700 °C in comparison to 0.86 Ω cm^2 for the undoped composition at the same temperature. These values of polarization resistance are one order of magnitude lower than those reported previously for a symmetrical cell made of LSGM as electrolyte and $La_{0.75}Sr_{0.25}Cr_{0.5}Mn_{0.5}O_{3-\delta}$ (LSCM) as cathode [33]. The activation energies for the polarization resistance are very similar, ranged between 1.2 and 1.5 eV.

For the CGO electrolyte, the best result is obtained for Ti-doping, with a value of 0.22 Ω cm^2 at 700 °C in air (Supplementary material Fig. S2). The activation energies for the polarization resistance ranged between 1.2 and 1.4 eV.

It should be commented that the efficiency of the electrodes depends on their intrinsic properties but other factors are also relevant. For instance, the microstructure (e.g. porosity and grain size) has a significant influence on the transport of gaseous species and the number of reaction sites, where the electrochemical reactions occur. The sintering temperature is another issue to be considered, because an adequate adherence of the electrodes with low interdiffusion of elements is required. In this work, all electrodes were sintered at the same temperature, 1100 °C, for comparison purpose, however the dopant has a significant influence on the densification and grain size, thus different sintering temperature of the electrodes possibly could enhance the polarization resistance values.

As mentioned in the phase stability section, the doped samples retain the cubic structure after annealing in a 5% H_2–Ar flow, and thus, their performance as anode material were tested. In Fig. 9b is shown the polarization resistance values in 5% H_2–Ar with LSGM electrolyte. The CGO electrolyte was not investigated due to its easy reduction at high temperatures under reducing conditions. The values of polarization resistance in 5% H_2–Ar are somewhat higher than those found in air with the best result for Zr-doping, with a value of 0.3 Ω cm^2 at 700 °C, which is comparable to LSCM symmetrical electrode [33]. The values of activation energy for the polarization resistance are somewhat lower than those found in air between 1.0 and 1.2 eV. This is due to the lower activity of the cathode for the oxygen reduction reaction at low temperature compared to the fuel oxidation in the anode.

On the other hand, there exists a clear relationship between the electrical conductivity, the polarization resistance and the ionic radii of the dopant (Fig. 10a). A maximum in the conductivity in air is observed for Ti-doping and as well as a minimum in the polarization resistance. Under hydrogen atmosphere (Fig. 10b), the conductivity decreases with the ionic radii of the dopant from 4.5 S cm^{-1} for Mo-doping to 0.4 S cm^{-1} for Zr-doping at 800 °C. The polarization resistance values also decreases with the ionic radii of the dopant from 0.8 Ω cm^2 for Mo-doping to 0.2 Ω cm^2 for Nb-doping at 800 °C.

In summary, these results obtained in this work suggest that doped strontium ferrites are alternative electrode materials to LSCM, for symmetrical SOFCs. However, different doping contents in $SrFeO_3$ should be studied to optimize the transport properties of these materials and improve the efficiency.

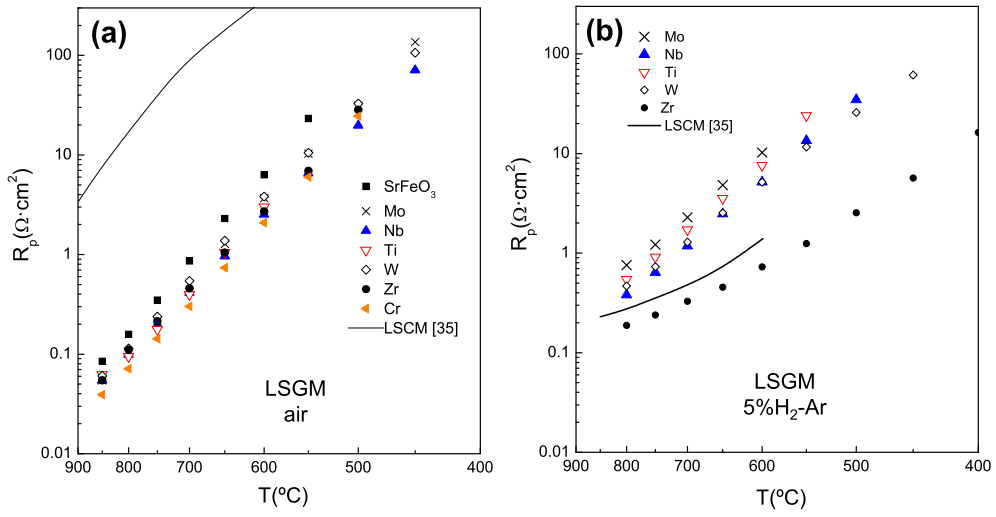

Fig. 9. Temperature dependence of the polarization resistance of $SrFe_{0.75}M_{0.25}O_{3-\delta}$ (M = Ti, Zr, Nb, Cr, Mo, W) electrodes deposited over the LSGM electrolyte in a) air and b) 5% H_2–Ar flow at open circuit conditions. The values of polarization resistance for $La_{0.75}Sr_{0.25}Cr_{0.5}Mn_{0.5}O_{3-\delta}$ (LSCM) [31] are also plotted for comparison purpose.

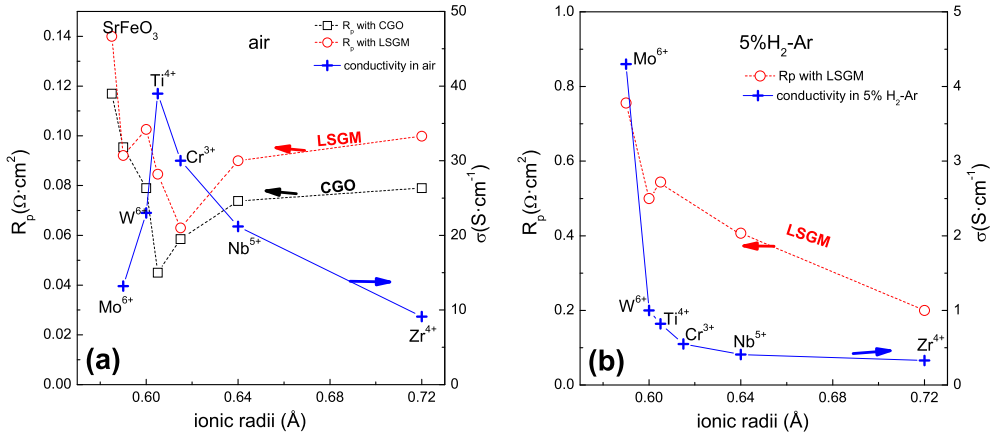

Fig. 10. Relationship between the area specific polarization resistance and the ionic radii of the dopant in $SrFe_{0.75}M_{0.25}O_{3-\delta}$ (M = Ti, Zr, Nb, Cr, Mo, W) with LSGM and CGO electrolyte in (a) air and (b) 5% H_2–Ar at 800 °C.

4. Conclusions

SFO and $SrFe_{0.75}M_{0.25}O_{3-\delta}$ (M = Cr, Mo, W, Nb, Ti and Zr) perovskite materials have been prepared by solid state reaction. Through doping a change from orthorhombic symmetry (with ordered oxygen vacancies) to a cubic one (with the oxygen vacancies disordered) is observed. Chemical compatibility studies with $Ce_{0.9}Gd_{0.1}O_{1.95}$ and $La_{0.8}Sr_{0.2}Ga_{0.8}Mg_{0.2}O_{3-\delta}$ showed no reactivity between them and the ferrites. Annealing experiments in 5% H_2–Ar showed the stabilization of the cubic form for the doped samples in reducing conditions, making them potentially suitable for anode applications. The electrochemical performance of the samples was examined on dense $Ce_{0.9}Gd_{0.1}O_{1.95}$ and $La_{0.8}Sr_{0.2}Ga_{0.8}Mg_{0.2}O_{3-\delta}$ pellets, the latter in two different atmospheres: air and 5% H_2–Ar. In both atmospheres an improvement in the area specific resistances (ASR) values were observed for the doped samples. Thus, these preliminary results show that high valence transition metals can be incorporated into perovskite materials and can have a beneficial effect on the performance, making them suitable for its use as cathode and anode materials in symmetrical SOFCs.

Acknowledgements

This work was supported by Junta de Andalucía (Spain) through the P10-FQM-6680 research grant and EPSRC (United Kingdom) through grant EP/I003932. We would also like to thank Prof. Maireles-Torres for fruitful discussions in XPS.

Appendix A. Supplementary data

Supplementary data related to this article can be found at http://dx.doi.org/10.1016/j.jpowsour.2013.10.118.

References

[1] N.P. Bansal, P. Singh, D. Singh, J. Salem, Advances in Solid Oxide Fuel Cells V, vol. 30, Willey, 2009.
[2] S.C. Singhal, K. Kendall, High Temperature Solid Oxide Fuel Cells: Fundamentals, Design and Applications, Elsevier, Oxford, 2004.
[3] B.C.H. Steele, A. Heinzel, Nature 414 (2001) 345–352.
[4] A. Orera, P.R. Slater, Chem. Mater. 22 (2010) 675–690.
[5] A.J. Jacobson, Chem. Mater. 22 (2010) 660–674.
[6] A. Atkinson, S.A. Barnett, R.J. Gorte, J.T.S. Irvine, A.J. McEvoy, M. Mogensen, S.C. Singhal, J. Vohs, Nat. Mater. 3 (2004) 17–27.
[7] J.W. Fergus, Solid State Ionics 177 (2006) 1529–1541.
[8] J.C. Ruiz-Morales, J. Canales-Vázquez, J. Peña-Martínez, D. Marrero-López, P. Núñez, Electrochim. Acta 52 (2006) 278–284.
[9] J.C. Ruiz-Morales, J. Canales-Vázquez, D. Marrero-López, D. Pérez-Coll, J. Peña-Martínez, P. Núñez, J. Power Sources 177 (2008) 154–160.
[10] J.C. Ruiz-Morales, D. Marrero-López, J. Canales-Vázquez, J.T.S. Irvine, RSC Adv. 1 (2011) 1403–1414.
[11] J. Canales-Vázquez, J.C. Ruiz-Morales, D. Marrero-López, J. Peña-Martínez, P. Núñez, P. Gómez-Romero, J. Power Sources 171 (2007) 552–557.
[12] Q. Liu, X. Dong, G. Xiao, F. Zhao, F. Chen, Adv. Mater. 22 (2010) 5478–5482.
[13] J. Yoo, A. Verma, S. Wang, A.J. Jacobson, J. Electrochem. Soc. 152 (2005) A497–A505.
[14] V. Zaspalis, A. Evdou, L. Nalbandian, Fuel 89 (2010) 1265–1273.
[15] Y. Niu, W. Zhou, J. Sunarso, L. Ge, Z. Zhu, Z. Shao, J. Mater. Chem. 20 (2010) 9619–9622.
[16] J.P. Hodges, S. Short, J.D. Jorgensen, X. Xiong, B. Dabrowski, S.M. Mini, C.W. Kimball, J. Solid State Chem. 151 (2000) 190–209.
[17] V.V. Vashuk, L.V. Kokhanovskii, I.I. Yushkevich, Inorg. Mater. 36 (2000) 79–83.
[18] M.V. Patrakeev, I.A. Leonidov, V.L. Kozhevnikov, V.V. Kharton, Solid State Sci. 6 (2004) 907–913.
[19] P. Adler, A. Lebon, V. Damljanovicacute, C. Ulrich, C. Bernhard, A.V. Boris, A. Maljuk, C.T. Lin, B. Keimer, Phys. Rev. B 73 (2006) 094451–094516.
[20] M. Schmidt, S.J. Campbell, J. Solid State Chem. 156 (2001) 292–304.
[21] A.C. Larson, R.B. von Dreele, GSAS Program, Los Alamos National Lab. Rep. No. LA-UR-86748, 1994.
[22] PANalytical BV, X'Pert HighScore Plus, Version 2.0a, 2004.
[23] Inorganic Crystal Structure Database (ICSD) v2008-01.
[24] D. Johnson, ZView: a Software Program for IES Analysis, Version 2.8, Scribner Associates, Inc., Southern Pines, NC, 2002.
[25] M. Amsif, D. Marrero-López, J.C. Ruiz-Morales, S.N. Savvin, M. Gabás, P. Nunez, J. Power Sources 196 (2011) 3461–3469.
[26] H. Falcón, J.A. Barbero, G. Araujo, M.T. Casais, M.J. Martínez-Lope, J.A. Alonso, J.L.G. Fierro, Appl. Catal. B Environ. 53 (1) (2004) 37.
[27] D. Marrero-López, J. Peña-Martínez, J.C. Ruiz-Morales, M. Gabás, P. Núñez, M.A.G. Aranda, J.R. Ramos-Barrado, Solid State Ionics 180 (2010) 1672–1682.
[28] A.A. Markov, M.V. Patrakeev, O.A. Savinskaya, A.P. Nemudry, I.A. Leonidov, O.N. Leonidova, V.L. Kozhevnikov, Solid State Ionics 179 (2008) 99–103.
[29] A.A. Markov, O.A. Savinskaya, M.V. Patrakeev, A.P. Nemudry, I.A. Leonidov, Yu.T. .Pavlyukhin, A.V. Ishchenko, V.L. Kozhevnikov, J. Solid State Chem. 182 (2009) 799–806.
[30] D. Marrero-López, J. Peña-Martínez, J.C. Ruiz-Morales, D. Pérez-Coll, M.C. Martín-Sedeño, P. Núñez, Solid State Ionics 178 (2007) 1366–1378.
[31] S. Tao, J. Irvine, Nat. Mater. 2 (2003) 320–323.
[32] J.C. Ruiz-Morales, J. Canales-Vázquez, D. Marrero-López, J.T.S. Irvine, P. Núñez, Electrochim. Acta 52 (2007) 7217–7225.
[33] J. Peña-Martínez, D. Marrero-López, D. Pérez-Coll, J.C. Ruiz-Morales, P. Núñez, Electrochim. Acta 52 (2007) 2950–2958.